System Modeling and Robust Control of an AMB Spindle: Part I Modeling and Validation for Robust Control

Hyeong-Joon Ahn
Department of Mechanical & Aerospace Engineering, University of Virginia, 122 Engineer's way, Charlottesville, Virginia 22904-4746, USA
Dong-Chul Han*
School of Mechanical & Aerospace Engineering, Seoul National University 151-745, Korea

This paper discusses details of modeling and robust control of an AMB (active magnetic bearing) spindle, and part I presents a modeling and validation process of the AMB spindle. There are many components in AMB spindle: electromagnetic actuator, sensor, rotor, power amplifier and digital controller. If each component is carefully modeled and evaluated, the components have tight structured uncertainty bounds and achievable performance of the system increases. However, since some unknown dynamics may exist and the augmented plant could show some discrepancy with the real plant, the validation of the augmented plant is needed through measuring overall frequency responses of the actual plant. In addition, it is necessary to combine several components and identify them with a reduced order model. First, all components of the AMB spindle are carefully modeled and identified based on experimental data, which also render valuable information in quantifying structured uncertainties. Since sensors, power amplifiers and discretization dynamics can be considered as time delay components, such dynamics are combined and identified with a reduced order. Then, frequency responses of the open-loop plant are measured through closed-loop experiments to validate the augmented plant. The whole modeling process gives an accurate nominal model of a low order for the robust control design.

Key Words: Modeling, Active Magnetic Bearing, Model Validation and Robust Control

Nomenclature

A : Area
B : Bandwidth of detector
C : Capacitance for current impulse
C_f : Feedback capacitor of detector
C_x : Unknown capacitance
$C^{nu\times 1}$: $nu\times 1$ dimension complex vector
f : Frequency
G : Transfer function of the plant
g_0 : Nominal air gap of electromagnetic actuator
i : Current
i_0 : Bias current of electromagnetic actuator
N_c : Number of coil turns
R_c : Coil resistance
R_f : Resistor for current measurement
R_{FET} : Turn on resistance of FET
T : Sampling time
U : Frequency response matrix of controller output
V_c : Charge voltage of capacitance detecting circuit
V_o : Output voltage of capacitance detecting circuit
V_s : DC link voltage for FET
Y : Frequency response matrix of controller input
Δ : Computation time
μ_0 : Permeability

* Corresponding Author,
E-mail: dchan@amed.snu.ac.kr
TEL: +82-2-880-7139; **FAX**: +82-2-883-1513
School of Mechanical & Aerospace Engineering, Seoul National University 151-745, Korea. *(Manuscript* **Received** July 4, 2002; **Revised** September 4, 2003)

ω : Frequency

1. Introduction

Active magnetic bearing (AMB) systems have been widely applied to exploit their unique advantages, including non-contact, lubricant-free operation, possibility of high rotational speed, and flexibility in choosing the bearing characteristics. AMB rotor systems always require feedback control of the magnetic force for stable levitation of the rotor. The dependence of magnetic force on the control variables is intrinsically nonlinear so an approximate linearized model, valid near an operating point, is used in design of the associated controller. As the result of the approximate nature of the model, careful modeling and validation of the actual system is essential in designing a high performance controller.

Robustness and reachable performance of the system are deeply related to an accurate nominal model. That is, if the system is precisely modeled and uncertainty bounds are very tight, the achievable performance of the system increases. In case of an AMB system, there are many components : magnetic bearing actuators, sensors, a rotor, power amplifiers and a digital controller. Therefore, the components should be modeled carefully to obtain an accurate nominal model for a high performance control design.

There are many works related to robust control. However, there are a few papers discussing details of modeling the components of an AMB system. Fittro (1998) applied the μ control to an AMB milling spindle, which contained detail modeling of the system and uncertainties and a performance weighting scheme. Also Losch et al. (1998) applied the μ control scheme to a 3 MW AMB boiler feed pump. This research described a model reduction method, a systematic way for uncertainty description, and a performance weighting scheme. However, even if the components are thoroughly modeled, some unknown dynamics may exist and the augmented plant could show some discrepancy with the real plant. Therefore, the validation of the augmented plant is needed through measuring overall frequency res ponses of the actual plant. In addition, it is necessary to combine several components and identify them with a reduced order model since the augmentation of the individual component models increases the system order considerably.

This paper discusses details of a modeling and validation process of an AMB spindle, which is the part I of the paper modeling and robust control of an AMB spindle. The AMB spindle of a new configuration is described and all components of the AMB spindle including rotor, sensors, electromagnetic actuators, power amplifiers, and discretization dynamics are carefully modeled and identified based on experimental data, which are also used in evaluating structured uncertainties of the components in part II. However, individual modeling and augmentation of the components lead to a very high order model. A useful compromise is adopted to separately identify these easily segregated effects and perform a reduced identification on them collectively. Then, frequency responses of overall open-loop plant are measured through closed-loop experiments to validate the augmented plant. The modeling and validation process renders an accurate model of a low order for the design of robust control in the part II.

2. AMB Spindle

There were two configurations of AMB spindles : two radial magnetic bearings (Siegwart, 1990) and three bearings (Stephens, 1995). The configuration of the two bearings is simple and gives a rigid rotor design, but may have weak observability or controllability of bending modes. The configuration of the three bearings has good controllability and observability of bending modes, but is intrinsically complex and gives lower bending natural frequency of the rotor.

Authors propose a new configuration, three sensors and two bearings. This configuration gives several advantages ; more rigid rotor and higher natural frequency than the three bearings design, higher modal observability than the configuration of the two bearings design, possibility to install a sensor system very close to a tool position and to measure radial and axial vibrations of the tool, and comparison of control performances between the conventional and new design through the interpolation of front two

Table 1 Specifications of the AMB spindle

Specifications	Value
Rotor mass	2.7 Kg
Max. rotational speed	60,000 rpm
Motor power	3 kw
Bearing diameter	39 mm
Air gap	0.30 mm
Max. radial force	200 N

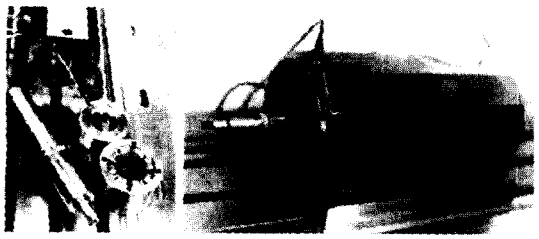

(a) Components (b) Assembly

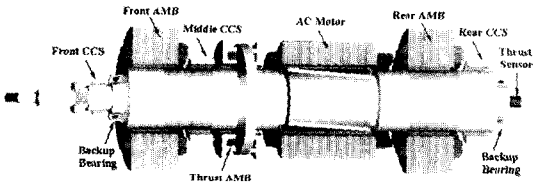

(c) Schematic

Fig. 1 The AMB spindle

sensors.

Experimental setup of the proposed configuration is shown in Fig. 1. The AMB rigid rotor experimental setup consists of two AMB units with a built-in cylindrical capacitive sensor (CCS), a thrust bearing, a rigid rotor, and a induction motor. The CCS and the electro-magnetic actuator are embedded in the AMB unit as shown in Fig. 1(a). Specifications of the AMB spindle are described in Table 1.

3. Modeling and Identification of Components of the AMB Spindle

3.1 Rotor dynamic modeling

Finite element method (FEM) is used in state-space modeling of the rotor through commercial software or RODAP (D&M Co., 2001). Here, the material of the rotor is considered as isotropic and linear elastic in order to get the linear time-invariant model. The FEM model of the AMB spindle consists of 27 elements and 35 nodes, as shown in Fig. 2. The bending diameters at the interference fit locations are adjusted ; light gray denotes bending diameter and dark gray denotes mass diameter.

Two bending modes are included in the rotor dynamic modeling considering controller bandwidth or 2 kHz, which is about one fifth of the

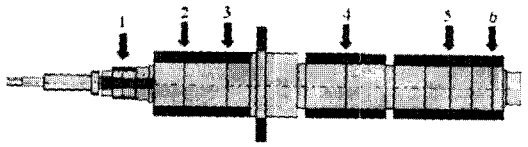

Fig. 2 FEM model of the spindle and node points for impulse test

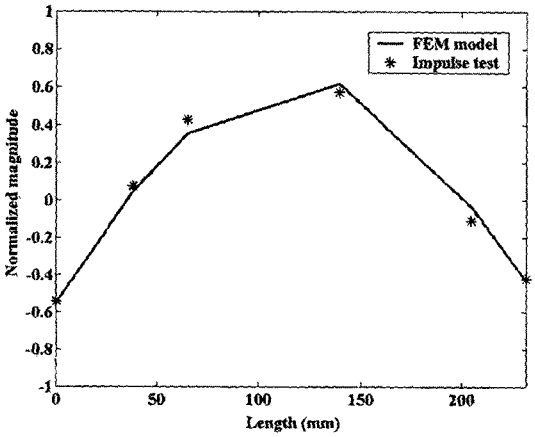

(a) The 1st bending mode

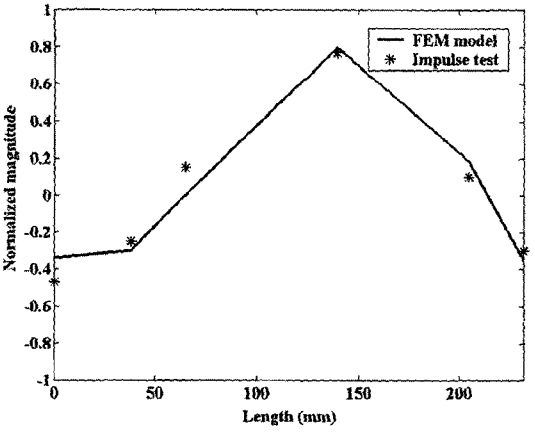

(b) The 2nd bending mode

Fig. 3 Mode shapes of the FEM model and impulse test

Table 2 Natural frequencies of the FEM model and impulse test

	FEM model	Impulse test
1st bending natural frequency (Hz)	1468.37	1468
2nd bending natural frequency (Hz)	2249.10	2248

sampling frequency.

Once a theoretical model is established, the next step is validation of the theoretical model with an impulse test. Six nodal points including bearing and sensor locations are chosen for the impulse test as shown in Fig. 2. The 1st, 3rd and 6th nodal points are the sensor locations while the 2nd and 5th nodal points are the bearing locations.

Normalized mode shapes of the FEM model and impulse test data are shown in Fig. 3. The bending natural frequencies of the FEM model and impulse test data are shown in Table 2. The FEM model matches very well with the impulse test result.

3.2 Sensor dynamic modeling and calibration

3.2.1 Sensor dynamics

Fundamental capacitance detecting circuit for the CCS is based on the charge transfer method and it can avoid interference between the sensor electrodes and achieve a high bandwidth (Huang et al., 1988). The circuit can be modeled considering several practical OP amplifier characteristics such as an open-loop gain and time constant. The resulting frequency response function is

$$G(\omega)=\frac{V_o(\omega)}{C_x(\omega)}=\frac{fV_cR_f}{(j\omega/\omega_{s1}-1)(j\omega/\omega_{s2}-1)} \quad (1)$$

where f is excitation frequency, V_c is the excitation voltage, R_f feedback resistor and ω_{s1} and ω_{s2} are the sensor system poles.

The static output voltage of the transducer is given by

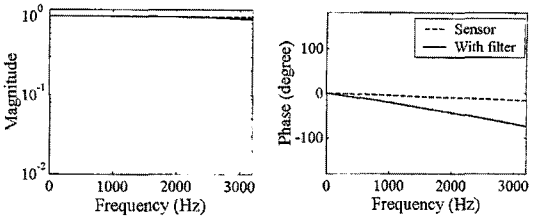

Fig. 4 Frequency responses of sensor dynamics

$$V_o=fV_cR_fC_x \quad (2)$$

If the unknown capacitance C_x is a function of the displacement x with very high bandwidth, Eq. (2) can be consider as the sensor dynamics. The calculated dominant system pole is $1/R_fC_f$, about 10 kHz. A second order Butterworth low pass filter with 5 kHz bandwidth is introduced to reduce noise. The frequency responses of the sensor and overall sensor dynamics including the low pass filter are shown Fig. 4.

3.2.2 Sensor calibration

The front sensor is the 8-segment CCS, and middle and rear sensors are the 4-segment CCSs (Ahn et al., 2000; Jeon et al., 2001). For simplicity, the nonlinear relationship between the displacement of a rotor and capacities is approximated in the CCS and the calibration procedure of the CCS is inevitable. Since a CCS measures rotor displacements in both X and Y directions at an axial measurement plane, the CCS should be calibrated in both directions at the same time. The calibration procedure of a CCS is as follows: First, the center of the CCS is set electrically through making the both directional outputs zero without any target. The sensor output is measured moving an alternative target with the same diameter as the spindle in both X and Y direction. The gain of the CCS is evaluated with the measured data.

The output of the CCS is measured with moving a target within $\pm 100\ \mu$m in both X and Y directions by the 10 μm step. Schematic of the sensor calibration experimental setup is shown in Fig. 5. Newport M462, XYZ stage equipped with micrometer is used.

The measured data with the front CCS is

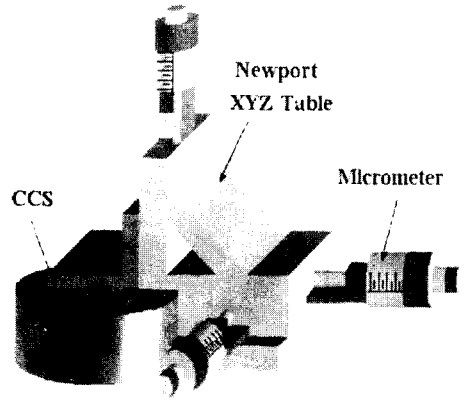

Fig. 5 Schematic of sensor calibration set-up

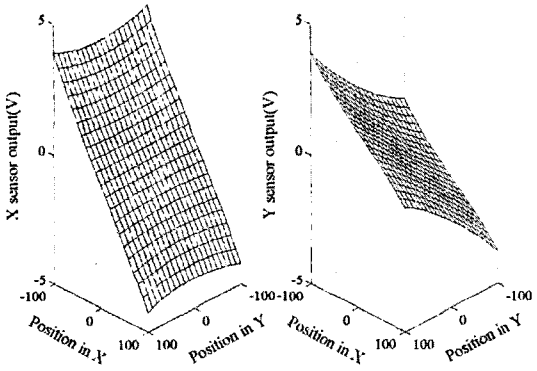

Fig. 6 Measured data of the front 8-segment CCS

shown in Fig. 6. The nonlinearity appears as the target goes far from the center position. The sensor calibration is performed within $\pm 70\ \mu m$ through the minimum zone criterion since 100 μm radius range in a polar coordinate can be approximated by $\pm 70\ \mu m$ in Cartesian coordinate. The additive and relative nonlinear errors are less than 2.5 μm and 2.5%, respectively. The simulation of the CCS calibration process is also performed using measured geometric data and a mathematical model of the CCS (Ahn et al., 2000). The simulated sensor gains match with the experimental ones within an acceptable error, as shown in Table 3.

3.3 Measurements of open-loop AMB properties

Although the magnetic force equation is nonlinear over a full operation range, the mathematical model can be linearized near an operating point and the linearized model is used to design a controller for most AMB applications. These linearized parameters: current gain and open-loop stiffness are quite sensitive to small variations in an operating point. Since these parameters govern the unstable poles of an AMB system, it is necessary to measure the nominal values accurately. In addition, structured uncertainties can be evaluated from measured actual AMB properties, which will be described in the part II.

Table 3 Calibration results of the CCSs

Sensor	Direction	Experimental gain (V/mm)	Theoretical gain (V/mm)
Front sensor	X	26.83	24.78
	Y	26.13	24.78
Middle sensor	X	35.87	34.30
	Y	35.08	34.30
Rear sensor	X	34.07	34.30
	Y	33.46	34.30

AMB in the experimental setup is heteropolar type bearing whose specifications are as follows: the number of coil turns is 270 per one pole leg, air gap is 0.3 mm, bias current is 0.4 A, and material is Si-steel. The saturation magnetic flux density is assumed to be 1.4 T considering a safety factor, and the bias current is determined about one third of bias current.

Current gain can be defined as a linearized gain from perturbation current to bearing force at the operating point $x=0$ and $i_c=0$. The current gain can be easily measured if successive forces are applied and the increased currents to maintain the zero position with a simple PID control are measured. The four 250 g forces are applied successively up to 1 kg force and the increased currents are measured in three times. The experimental data of the front bearing is shown in Fig. 7. A least square fitting is adopted to obtain an approximate current gain. Hysteresis effect gives small offset of initial current value between loading and unloading forces. There are a notable

difference between measured and theoretical current gains are shown in Table 4, which is due to coating for electric insulation and leakage of magnetic flux.

Open-loop stiffness can be described as a linearized stiffness from perturbation position to bearing force at the operating point $x=0$ and $i_c=0$. The open-loop stiffness can be measured if successive forces are applied and the changes of positions to prevent the variation of perturbation current with a simple PID control are measured. The four 250 g forces are applied successively up to 1 kg force and the positions to maintain the initial current value are measured at four different angle location of the spindle. The experimental data of the front bearing are shown in Fig. 8. Approximated open-loop stiffness is obtained with a least square fitting. The open-loop stiffness is very sensitive to an initial position, which means that the small change of the angle location of the spindle perturbs the open-loop stiffness due to the run-out of the rotor. The measured and theoretical open-loop stiffness is shown in Table 5.

Table 4 Measured and theoretical current gain

	Front Bearing	Rear Bearing
Theory (N/A)	287.46	287.46
Experiment (N/A)	225.16	212.2

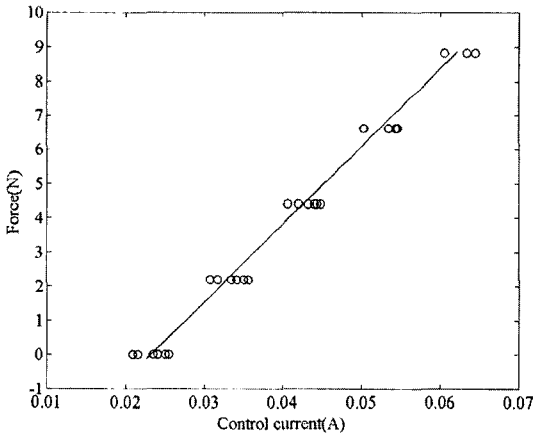

Fig. 7 Experimental evaluation of current gain

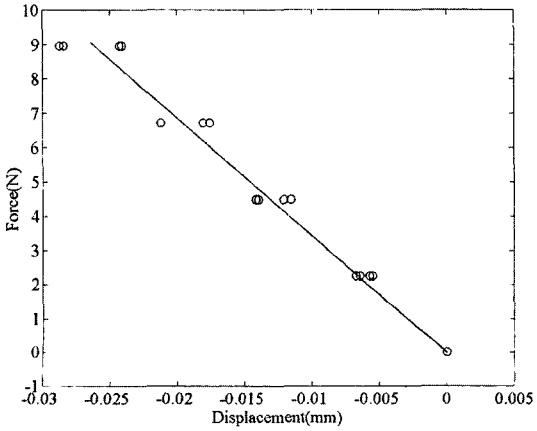

Fig. 8 Experiment evaluation of open-loop stiffness

3.4 Power amplifier

A simple linear amplifier made of operational amplifiers and FETs (IRF 150) was used for the AMB spindle. Frequency response of the power amplifier was measured using a sine chirp signal of the HP 35670A dynamic analyzer. The excitation signal was added to a control signal of the AMB actuator and the frequency response from the control signal to current of the AMB actuator was measured. Then, the measured frequency response was fitted with a third order model using a least squares algorithm (Sanathanan and Koerner, 1963). The measured and fitted frequency responses of the power amplifier are shown in Fig. 9.

Table 5 Measured and theoretical open-loop stiffness

	Front Bearing	Rear Bearing
Theory (N/mm)	342.68	342.68
Experiment (N/mm)	340.45	415.48

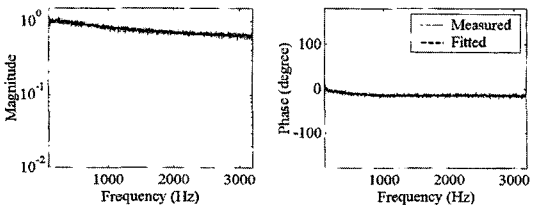

Fig. 9 Measured and fitted frequency responses of the power amplifier

3.5 Modified design of continuous controllers considering discretization (Lewis, 1992)

There are some considerations involved in a digital controller; sampling and hold operations, a computation delay, and an anti-aliasing filter. The modified continuous design of a controller denotes that a continuous controller is designed considering several effects of the discretization. Its disadvantage is that the sampling period must be selected prior to the continuous controller design. The advantage of the approach is that the effects of the sampling and hold operations, computation delay, and aliasing filter are included and compensated for in the controller design stage.

3.5.1 Anti-aliasing filters

As long as the sampling frequency is selected at least twice as large as the plant cut-off frequency, the effects of the aliasing will be small. However, high-frequency measurement noise may be aliased down to lower frequencies within the plant bandwidth and thus have a detrimental effect on system performance. To avoid this, low-pass anti-aliasing filters may be inserted after the measuring devices and before the samplers. The cut-off frequency should be selected less than half of the sampling frequency so that there is good attenuation beyond the plant bandwidth. If the cut-off frequency of the anti-aliasing filter is not much higher than the plant cut-off frequency, the filter will affect the closed-loop performance, and it should be appended to the plant at the design stage.

Anti-aliasing filters that have 6 poles and 50 kHz bandwidth were already equipped in the data acquisition hardware. Bandwidth of the anti-aliasing filter is too high considering sampling frequency. Therefore, the effect of anti-aliasing filters on the system dynamics is negligible.

3.5.2 Computation delay dynamics

The delay associated with a computation time of Δ has a transfer function of

$$G_{delay}(s)=e^{-s\Delta} \tag{3}$$

which has a magnitude of one and a phase of $-\omega\Delta$ radians. To account for this delay, the continuous controller design may be performed not on the plant $G(s)$, but on $G(s)e^{-s\Delta}$. However, since the model of Eq. (3) has infinite dimension, it is required to approximate the delay with a rational transfer function.

For this purpose, we may use Pade approximation (Lewis, 1992) to $G_{delay}(s)=e^{-s\Delta}$, which match the first few terms of the Taylor's series expansion. Note that the Pade approximation with finite zeros is non-minimum phase, which is a property of the pure time delay.

3.5.3 Zero order hold (ZOH) and sampler dynamics

Since the sampler has a gain of $1/T$, the sampler plus ZOH has a transfer function of

$$G_{zoh}=(1-e^{-sT})/sT \tag{4}$$

These have been computed using the Pade approximations of e^{-sT}. Although they are not, strictly speaking, the Pade approximations, they are, however, sufficiently accurate in an acceptable accuracy. Note that the approximation of ZOH has unstable zeros also.

3.5.4 Overall discretization dynamics

For verification of the dynamic models for the discretization dynamics, frequency response of a digital controller is measured with just echo, that is, the digital controller plays a role as a wire. The sampling frequency is 10 kHz and the time delay is assumed about 0.1 msec. The 3^{rd} order all-pass Pade approximations are used for both computation delay and ZOH. Measured and expected frequency responses of the discretization

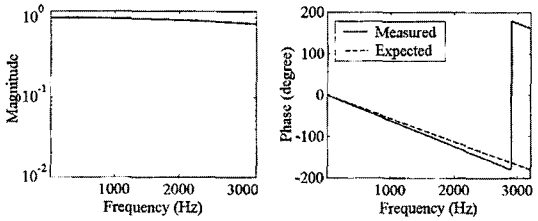

Fig. 10 Measured and expected frequency responses of the discretization dynamics

dynamics are shown in Fig. 10. Although the magnitude matches very well, the phase doesn't match very well. This comes from an additional small time delay in AD/DA conversion, which is hardly estimated since it depends on the hardware and software implementations. The measured discretization dynamics is fitted as a third order model through the least square algorithm.

4. Measurement of Open-Loop Frequency Responses

4.1 Introduction

Even if the components are thoroughly modeled in sec. 3, some unknown dynamics may exist and the augmented plant could show some discrepancy with the real plant. Therefore, the validation of the augmented plant is need through measuring overall frequency response of the real plant. Frequency responses of an AMB system can be measured without any extra hardware, if a digital control is used (Ha and Lee, 1997). Excitation and data acquisition can be implemented in the software of the digital controller. This procedure can provide a more accurate nominal model especially for a control design, since measurements are done through the signals that the controller is using.

Since an AMB system is open-loop unstable, all experiments must be performed in closed-loop. The general closed-loop AMB system is shown in Fig. 11. The averaged frequency spectra of input vector u and output vector y are used to get the frequency response function (FRF) of the plant as shown in Fig. 13. The frequency spectra vectors of input and output signal vectors are $U^{(i)}(j\omega) \in C^{nu\times 1}$, $Y^{(i)}(j\omega) \in C^{ny\times 1}$, $i=1, 2, \cdots, N_{exp}$. Here, nu, ny are the number of inputs and outputs, and N_{exp} is the number of experiments, respectively. Defining the input/output data matrices at the frequency ω as

$$Y(j\omega) = [\, Y^{(1)}(j\omega)\ Y^{(2)}(j\omega) \cdots Y^{(Nexp)}(j\omega)\,]^T \in C^{ny\times Nexp} \quad (5)$$

$$U(j\omega) = [\, U^{(1)}(j\omega)\ U^{(2)}(j\omega) \cdots U^{(Nexp)}(j\omega)\,]^T \in C^{nu\times Nexp} \quad (6)$$

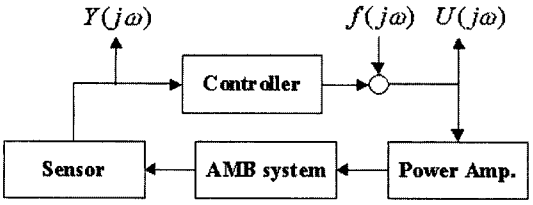

Fig. 11 System block diagram for the measurement of frequency response of open plant FRF

Then non-parametric transfer function matrix $G(j\omega) \in C^{ny\times nu}$ can be obtained by (Pintelon et al., 1998)

$$G(j\omega) = Y(j\omega)\, U(j\omega)^{+} \quad (7)$$

Here superscript + denotes the Moore-Penrose pseudo-inverse.

The frequency responses measured in a digital controller include all dynamics of a plant such as sensors, power amplifiers and discretization dynamics except the controller, which give us a useful for the validation of the augmented plant model. Also, repeated measurement of the open-loop frequency responses shows the necessity of introducing several structured and unstructured uncertainties of the plant.

4.2 Measuring methodology

The system is excited with a single-frequency sinusoidal signal to get frequency responses of a good quality although required testing and computation time is so big.

In general, amplitude of an excitation signal should be as large as possible to ensure sufficient signal-to-noise ratio. Except for safety or economic reasons, there are two important factors that limit amplitude of the excitation signal for an AMB system : linear region and slew rate of an electromagnetic actuator. The linearity region limits the excitation range to approximately one third of the nominal gap g_0— less than 100 μm. The current slew rate limitation restricts the amplitude of the excitation signal with a given sampling time. The current slew rate of the magnetic bearing rotor system is described by

$$\frac{di}{dt} = \frac{2g_0}{\mu_0 N_c^2 A}\left[\, V_s - (i_b + i)\,(R_c + R_f + R_{FET})\,\right] \quad (8)$$

Here, V_s is the supply voltage (60 V), R_c the coil resistance (0.4 Ω), R_f the resistor connected to FET (1 Ω), and R_{FET} the FET resistance (approximately 0.1 Ω). Considering these restrictions, the maximum amplitude of the excitation up to 3 kHz is limited to about 0.1 A.

4.3 Experimental results

5000 data with 10 kHz sampling frequency with a simple PID control are captured at each excitation frequency to calculate DFT of the captured data. Data of initial 0.1 sec is discarded for a transient vibration and 0.2 sec between each excitation is introduced for settling vibration. A total of six controller inputs and four actuator outputs are measured in each excitation ensemble. In addition, there are four such ensembles at each frequency and sinusoidal excitation is performed from 1 to 2999 Hz in 2 Hz step. The input and output data are captured in the control routine during an excitation, and the DFT of the captured data is calculated and stored in intermediate time between the time critical routines for data reduction. The measured closed-loop responses: controller input matrix (from $Y11$ to $Y33$) and actuator input matrix (from $U11$ to $U22$) in the X direction are shown in Fig. 12, which were described in Fig. 11. The two rigid modes appear below 1 kHz and a substructure mode appears near the second rigid mode.

Frequency responses of the open-loop plant can be calculated using Eq. (7). Since the AMB spindle is designed with as small diameters as possible to increase the maximum rotational

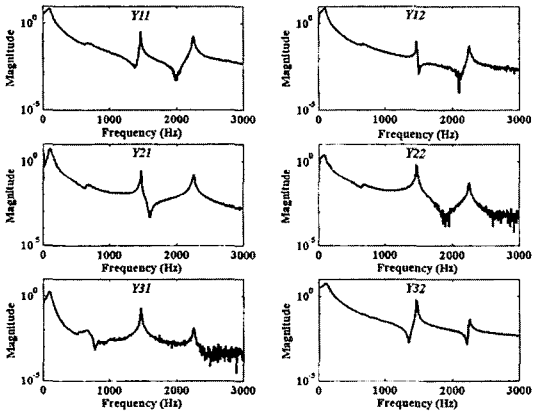

(a) Controller input matrix

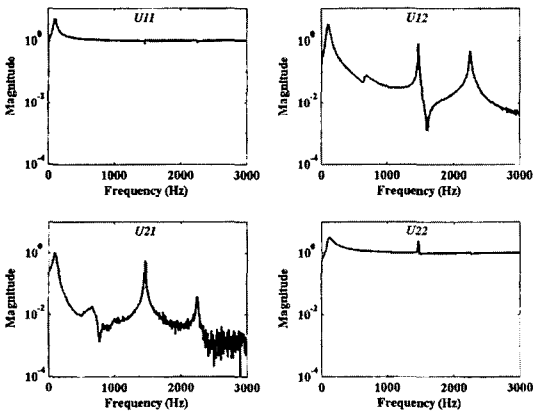

(b) Actuator input matrix

Fig. 12 Measured closed-loop responses in X direction

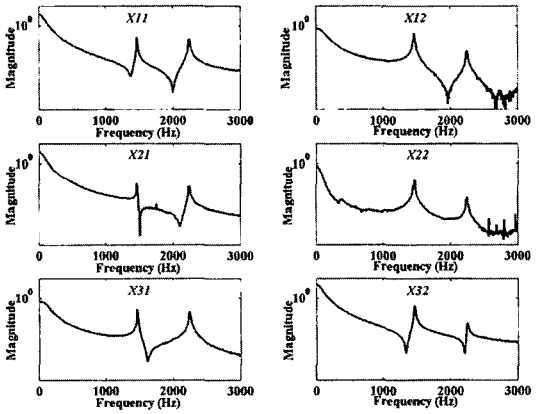

(a) Magnitude

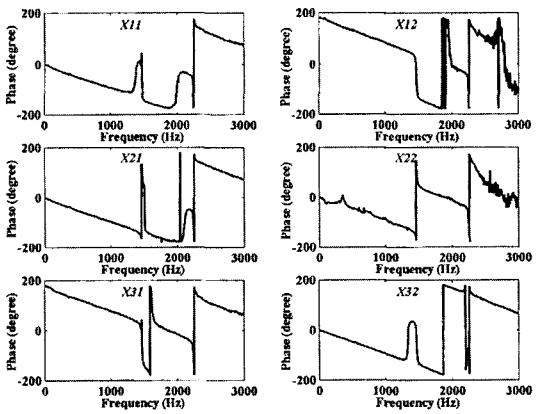

(b) Phase

Fig. 13 Calculated frequency responses in Y direction

speed, gyroscopic effect is negligible and coupling of the responses between X and Y directions is very small. The frequency response matrix is measured in 10 times and averaged. The calculated frequency response matrices in Y direction are shown in Fig. 13. The rigid modes and substructure dynamics of the closed-loop frequency responses disappear and the effect of the additional dynamics appears as a phase lag proportional to frequency. The frequency response matrices in X and Y directions are almost identical except the small difference in the magnitude and substructures. In general, the substructure can be modeled with simple second order or mass spring damper systems. However, the effects of substructure dynamics are so small that we can ignore them in this paper.

5. Model Validation

5.1 Augmentation

All components identified and modeled before are augmented, and the theoretical model has 35 poles. Such a high order model renders a very high order controller, which means the difficulties in implementing the controller. Since most components behave like time delay components, they can be combined and identified with a reduced order model. The additional dynamics including discretization, sensor and power amplifier are combined and fitted with a third order model as shown in Fig. 14. The order of total delay dynamics is reduced from 10 to 3, which makes the system order 14.

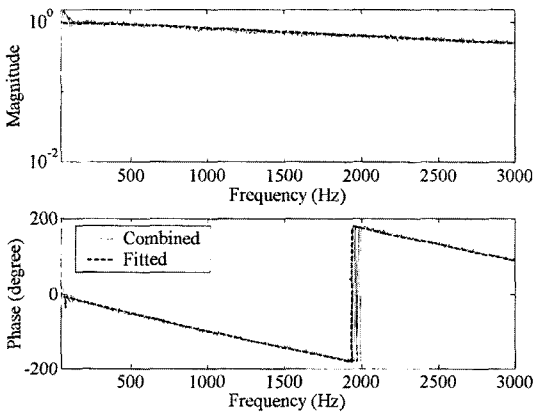

Fig. 14 Combined and fitted frequency responses of the additional dynamics

4.2 Model validation

Calculated frequency responses of the augmented theoretical model are compared with the measured frequency response matrix in X direction as shown in Fig. 15. The measured frequency responses agree well with the augmented theoretical model. There are some mismatches in slopes of X_{11}, X_{21} and X_{31} before the first bending mode, which mean a little bit difference between the measured and actual open-loop stiffness of the front AMB. In addition, there are inconsistencies in zero locations, which mean differences between eigenvectors of the model and the real

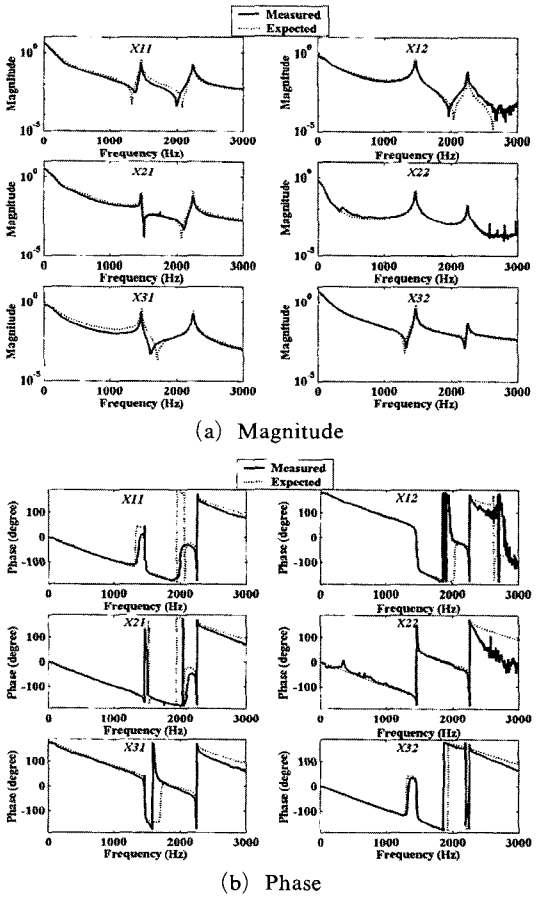

(a) Magnitude

(b) Phase

Fig. 15 Comparison of measured and expected frequency responses

rotor.

6. Conclusion

This paper discussed details of modeling and validation process of an AMB spindle. All components of the AMB spindle including rotor, sensor, electromagnetic actuator, power amp liter, and discretization dynamics were carefully modeled and identified through measuring frequency response of each component. The components such as sensor, power amplifier and discretization dynamics were combined and identified with a reduced order. Then, frequency responses of the open-loop plant are measured through on-line closed-loop experiments to validate the augmented whole plant. The whole modeling and validation process renders an accurate model of a low order for a robust control.

References

Ahn, H. J., Jeon, S. and Han, D. C., 2000, "Error Analysis of the Cylindrical Capacitive Sensor for Active Magnetic Bearing Spindles," *J. of Dynamics systems, measurement, and control*, trans. of ASME, March, Vol. 122, pp. 102~107.

D&M Technology Co., 2001, RODAP , Korea.

Fittro, R. L., 1998, "A High Speed Machining Spindle with Active Magnetic Bearings : Control Theory, Design, and Application," Ph. D. dissertation, University of Virginia.

Ha, Y. H. and Lee, C. W., 1997, "In-situ Modal Testing and Parameter Identification of Active Magnetic Bearing System by Magnetic Force Measurement and the Use of Directional Frequency response functions," *Transactions of KSME A.*, Vol. 21, No. 7, pp. 1156~1165.

Huang, S. M., Green, R. G., Plaskowski, A. and Beck, M. S., 1988, "A High Frequency Stray-immune Capacitance Transducer based on the Charge Transfer Principle," *IEEE Transactions on Instrumentation and Measurement*, Vol. 37, No. 3, pp. 368~373.

Jeon, S., Ahn, H. J., Chang, I. B. and Han, D. C., 2001, "A New Design of Cylindrical Capacitive Sensor for On-line Precision Control of AMB Spindle," *IEEE Transactions on Instrumentation and measurement*, Vol. 50 No. 3, pp. 757~763.

Lewis, F., 1992, Applied Optimal Control & Estimation, Prentice-Hall International, Inc.

Losch, F., Gahler, C. and Herzog, R., 1998, "μ-Synthesis Controller Design For a 3MW Pump Running In AMBs," *Proceedings of the 6th ISMB*, MIT, Massachusetts, USA, pp. 415~428.

Pintelon, R., Guillaume, P., Vandersteen, G. and Rolain, Y., 1998, "Analyses, Development, and Applications of TLS Algorithms in Frequency Domain System Identification," *SIAM J. Matrix Anal. Appl.*.

Sanathanan, C. K. and Koerner, J., 1963, "Complex Function Synthesis as a Ratio of Two Complex Polynomials," *IEEE Transaction of Automatic Control*, AC-8, 37.

Siegwart, R., Larsonneur, R. and Traxler, A., 1990, "Design and Performance of a High Speed Milling Spindle in digitally Controlled Active Magnetic Bearings," *Proceedings of the 2nd ISMB*, Tokyo, Japan, pp. 197~204.

Stephens, L. S., 1995, "Design and Control of Active Magnetic Bearings for a High Speed Machining Spindle," Ph. D. dissertation, University of Virginia.